Steven Adler-Golden, David Less, Xuemin Jin, and Peter Rynes “Modeling and analysis of LWIR signature variability associated with 3D and BRDF effects," SPIE Proceedings Volume 9840, Algorithms and Technologies for Multispectral, Hyperspectral, and Ultraspectral Imagery XXII; 98400P (2016).

DOI: https://doi.org/10.1117/12.2224115

See next page for full paper.

Modeling and analysis of LWIR signature variability associated with 3-D and BRDF effects

Steven Adler-Golden*[a], David Less[b], Xuemin Jin[a] and Peter Rynes[b]
[a]Spectral Sciences, Inc., 4 Fourth Avenue, Burlington, MA USA 01803-3304
[b]ThermoAnalytics, Inc., 23440 Airpark Blvd., Calumet, MI USA 49913

ABSTRACT

Algorithms for retrieval of surface reflectance, emissivity or temperature from a spectral image almost always assume uniform illumination across the scene and horizontal surfaces with Lambertian reflectance. When these algorithms are used to process real 3-D scenes, the retrieved "apparent" values contain the strong, spatially dependent variations in illumination as well as surface bidirectional reflectance distribution function (BRDF) effects. This is especially problematic with horizontal or near-horizontal viewing, where many observed surfaces are vertical, and where horizontal surfaces can show strong specularity. The goals of this study are to characterize long-wavelength infrared (LWIR) signature variability in a HSI 3-D scene and develop practical methods for estimating the true surface values. We take advantage of synthetic near-horizontal imagery generated with the high-fidelity MultiService Electro-optic Signature (MuSES) model, and compare retrievals of temperature and directional-hemispherical reflectance using standard sky downwelling illumination and MuSES-based non-uniform environmental illumination.

Keywords: long wavelength infrared, hyperspectral, temperature-emissivity separation, BRDF, specular, MuSES

INTRODUCTION

Long-wavelength infrared (LWIR) hyperspectral imagery (HSI) has significantly improved in quality and availability in recent years, sparking interest in a variety of remote sensing applications, such as characterizing surface composition and temperature and detecting chemicals and gas plumes. The exploitation of LWIR HSI technology is however less well developed than for visible through short wavelength infrared (SWIR) HSI, where radiation is from the sun rather than from thermal emission. Quantitative retrieval of surface temperatures and emissivities from LWIR HSI has been demonstrated using both first principles methods[1-4] and a semi-empirical, in-scene method[5] for the relatively simple case of horizontal surfaces and downward viewing under a clear sky. Here illumination is entirely from atmospheric downwelling radiation, and the favorable viewing geometry limits specularity effects for most non-metallic materials.

The surface retrieval problem is much more challenging in near-horizontal views, where both tops and sides of objects are seen. The tops are viewed at glancing angles, where the material bidirectional reflectance distribution functions (BRDFs) are often strongly specular, and the sky background reflected by these surfaces is enhanced by limb brightening. The sides of the objects are illuminated not only by the sky but also by the ground and nearby objects, making the spectra more blackbody-like and thus less spectrally distinct. Under these viewing conditions, standard LWIR HSI retrieval algorithms are unable to derive quantitative emissivities and temperatures. However, the problem is solvable, at least in principle, with model predictions or measurements of the illumination spectrum at each image pixel.

In this paper we use a synthetic 3-D LWIR HSI scene to demonstrate reflectance (1-emissivity) and temperature retrievals using pixel-specific illumination modeling, and we compare the results with those from a conventional retrieval. The pixel-specific modeling is essentially a closure experiment, as both the forward modeling code, MuSES[6,7], and the retrieval code, Fast Line-of-sight Atmospheric Analysis of Spectral Hypercubes - InfraRed (FLAASH-IR)[3,4], use the same MODerate resolution TRANsmission (MODTRAN5®)[8] radiative transfer model. However, differences in the ways that these codes parameterize the atmosphere, as well as imperfect temperature-emissivity separation (TES), lead to some differences between inputs and retrievals. The largest differences reveal inherent sensitivities in the retrieval process, and mimic, in a milder form, uncertainties that might be expected when using 3-D modeling to analyze real imagery. For this scene, the reflectance retrievals using the standard FLAASH-IR downwelling spectrum show much larger errors, although the surface temperatures are usually correct to within a few degrees.

* adlergolden@spectral.com; phone 781 273-4770; fax 781 270-1161; spectral.com

CALCULATIONS

Scene Simulation

The Thermoanalytics, Inc. MultiService Electro-optic Signature (MuSES) code[6,7] performs first-principles calculations of thermal HSI images of 3-D scenes. Objects are defined via wireframe meshes to which optical properties (BRDFs) and thermal properties are assigned. The BRDFs are parameterized using the Sandford-Robertson model.[9,10] MuSES computes surface temperatures using a time-dependent heat transfer calculation incorporating convection, conduction, and radiation. The radiance emanating from a surface is the sum of thermal emission and reflected environmental radiance components. In this context, environmental radiance includes radiance from the sky, terrain, other surfaces of the object, and surrounding objects. MuSES computes an infinite-bounce value for the radiance reflected off other surfaces using spectral methods that vary with rendering application. The sky downwelling radiation is calculated using MODTRAN5. MODTRAN5 is also used to calculate the transmission and path radiance from each surface to the sensor.

For this work, we assembled an outdoor scene with a pond in the foreground and a building in the background. The surface temperature image is shown in Figure 1. The sensor is 500 m from the center of the scene and 50 m above the ground. The ground includes soil, grass, an asphalt road, and volcanic material on a low hill and on a flat area. The building has several different surface materials, including glass. In front of the building there are two boxes made of 10% Lambertian reflective material but at varying temperatures. The thermal radiance spectra for each pixel were calculated over the 8-14 micron range with 86 triangular instrument functions spaced 5 cm^{-1} apart.

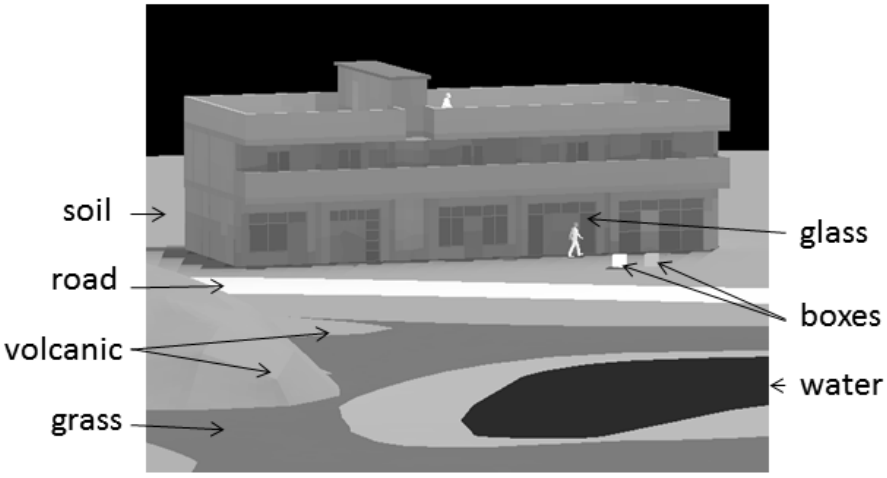

Figure 1. Temperature image of the MuSES scene. Grayscale corresponds to a temperature range of 290 K (black) to 320 K (white).

Environmental Radiance

The equation for at-sensor LWIR spectral radiance at wavelength λ, elsewhere written in the Lambertian reflectance approximation[3,4], generalizes to

$$L = \tau B(T)\big(1-\rho(\theta)\big) + \int d\theta_r \sin\theta_r \int d\varphi_r F(\theta,\theta_r,\varphi_r) I(\theta_r,\varphi_r)\cos\theta_r + U \qquad (1)$$

for surfaces described by a BRDF, denoted $F(\theta,\theta_r,\varphi_r)$. Here τ is the surface-to-sensor atmospheric transmission, $B(T)$ is the Planck function of surface temperature T, ρ is the directional hemispherical reflectance (DHR), I is the product of the environmental radiance and a transmission factor, and U is the atmospheric path radiance. Equation (1) is compatible with MODTRAN and other band model radiative transfer treatments, if one allows the transmission factor for the second term to differ from that for the first term, τ, accounting for differences in the spectral radiance fine structure. For consistency with other notation we refer to the angle between the surface normal and the line of sight (LOS) as the "incident" polar angle, θ, and the polar and azimuth angles associated with the incoming environmental radiation as the "reflected" angles θ_r and φ_r, respectively. We assume that the surfaces have no striae or other oriented marks, so the

BRDF's azimuthal dependence incorporates only the difference between the incident and reflected azimuth angles, and we choose a fixed incident azimuth angle. The DHR is the BRDF integrated over the hemisphere above the surface:

$$\rho(\theta) = \int d\theta_r \sin\theta_r \int d\varphi_r F(\theta_i, \theta_r, \varphi_r) \cos\theta_r \tag{2}$$

The DHR for the Sandford-Robertson BRDF model has an analytical form.[10]

It would be extremely cumbersome to formulate and retain the (θ_r,φ_r) dependence of the environmental radiance at every pixel and wavelength. Instead, we define an "effective" environmental radiance, D_e, based on a factored representation of the second term in Equation (1):

$$\int d\theta_r \sin\theta_r \int d\varphi_r F(\theta, \theta_r, \varphi_r) I\left(\theta_r, \varphi_r\right) \cos\theta_r = \rho(\theta) D_e \tag{3}$$

Note that D_e, like L, is an HSI data cube. D_e depends on the surface BRDF's (θ_r,φ_r) dependence, but it is independent of the reflectance magnitude. Therefore an estimate of D_e obtained from a single MuSES scene simulation would be applicable to a family of surfaces with similar levels of specularity but different absolute reflectances.

The environmental illumination calculations performed in MuSES are not currently output by the code. Therefore we derived D_e using Equations (1) and (2) by starting from the output radiance image, L, subtracting U and the transmitted surface thermal emission (the first term in Equation (1)), and dividing the result by $\rho(\theta)$. Since the distances between objects in the scene are smaller than the distance to the sensor, the atmospheric components τ and U vary only slightly across the scene. We used average values of these quantities obtained by running FLAASH-IR on the MuSES radiance image. The results were very close to MODTRAN5 calculations for the sensor-to-scene-center LOS using the MuSES model atmosphere. The surface thermal emission component was calculated from maps of material type, surface temperature and range (distance to the surface) used in the radiance simulation. We note that as $\rho(\theta)$ approaches zero, this method for deriving D_e becomes inaccurate, but at the same time D_e becomes unimportant for temperature and emissivity retrievals.

FLAASH-IR Retrievals

The original version of the Spectral Sciences, Inc. FLAASH-IR algorithm solves the radiance equation (1) for horizontal Lambertian surfaces and scene-average atmospheric spectra. In this simplified model, D_e is the transmitted sky downwelling flux, denoted D. Detailed descriptions of FLAASH-IR are given elsewhere.[3,4] Trial atmospheres are modeled by starting from a layered approximation to a standard MODTRAN model atmosphere and forming a look-up table (LUT) by modifying the temperature, water vapor and ozone profiles. The retrieved atmospheric τ, U and D spectra are interpolates from this 3-D LUT that minimize a total in-band squared radiance error σ^2 summed over a selected set of i diverse pixels:

$$\sigma^2 = \sum_{i\lambda} [L_{iobs} - L_i(\langle\varepsilon\rangle)]^2 \tag{4}$$

Here ε denotes spectral emissivity, and

$$L(\langle\varepsilon\rangle) = B(T)\langle\varepsilon\rangle\tau + (1 - \langle\varepsilon\rangle)D + U \tag{5}$$

where $\langle \quad \rangle$ denotes spectral smoothing with a running average. That is, the quantity to be minimized is a measure of the difference between the actual pixel radiances and the radiances calculated from smoothed emissivities, where the emissivities pertain to a trial atmosphere and trial pixel temperatures. Once the atmosphere is retrieved, the temperature and emissivity or reflectance images are obtained by minimizing the radiance error with respect to T for each pixel in the scene.

For the current work, we prototyped a new, more general version of FLAASH-IR, in which D is replaced by the D_e data cube in the TES step. With this modification, the retrieved reflectance, 1-ε, is the DHR, and can be directly compared with the DHR of the surface input to MuSES.

While the D_e replacement in FLAASH-IR is straightforward, a complication is that D_e associated with a 3-D environment can be much larger than the transmitted sky downwelling D, and thus may approach, or even exceed, the value $\tau B(T)$. When these quantities are equal—i.e., the brightness temperature of the environmental illumination matches that of the surface—the emissivity solution, below, becomes indeterminate:

$$\varepsilon = (L - D_e - U)/(\tau B(T) - D_e) \tag{6}$$

The indeterminacy results in unstable retrievals at certain wavelengths, emissivities and temperatures. The instability can in turn cause a problem in calculating $\langle\varepsilon\rangle$, the spectrally smoothed emissivity, when it occurs at wavelengths within the averaging window. Fortunately, this last problem can be mitigated: we formulate $\langle\varepsilon\rangle$ as a linear regression slope, for which the solution is

$$\langle\varepsilon\rangle = \langle(L - D_e - U)(\tau B(T) - D_e)/(\tau B(T) - D_e)^2\rangle \tag{7}$$

With this expression, a brightness temperature mismatch at any wavelength within the averaging window assures a stable value of $\langle\varepsilon\rangle$.

RESULTS

Table 1 compares input material temperatures ("true") with FLAASH-IR retrieved temperatures for various locations in the MuSES scene. With the sky radiance, D, as the illumination source, the temperatures are generally accurate to within a few degrees. Using D_e from MuSES instead brings the temperatures into much closer agreement with the true values—within 0.3 degrees or less in five out of the seven locations. The most notable exception is the "volcanic flat" area (the upper arrow in Figure 1), where the combination of a specular material and low viewing angle makes the DHR very large, around 0.9. With the low emissivity of ~0.1, the surface emission is small compared to the atmospheric contributions to the radiance, making the surface temperature poorly determined. This difficulty in remotely sensing temperatures of reflective surfaces is a general one, regardless of the sources of illumination. In contrast, the "volcanic hill" surface (the lower arrow in Figure 1) is viewed at a higher angle, resulting in a lower DHR and higher emissivity (around 0.3), and therefore a much more accurate temperature retrieval.

Table 1. Comparison of true and retrieved surface temperatures (K) for the MuSES image.

Material	Pixel x,y location	True	FLAASH-IR (sky D illumination)	FLAASH-IR (MuSES D_e illumination)
glass	353,239	300.9	303.5	300.9
grass	318,354	304.4	304.1	304.4
left box	486,264	328.2	324.9	328.5
volcanic hill	107,347	310.8	311.5	311.1
volcanic flat	154,330	310.7	313.9	314.3
road	354,293	319.4	317.2	318.0
water	533,401	294.8	299.6	294.8

Figures 2 and 3 show DHR spectrum comparisons for these same locations. For around half the surfaces, the simple retrieval based on the sky illumination, D, reasonably preserves the spectral shape, although the absolute reflectivities are too low. This is in accord with a previous paper on FLAASH-IR[3], in which using D for vertical surface retrievals resulted in reflectance spectra that appeared to be around a factor of two too low but reasonable in shape. In the current scene, the differences between using D and the MuSES-derived D_e are much more dramatic for some surfaces, such as glass. The extreme specularity and vertical orientation of the glass result in a large D_e, in which the illumination originates from the sky and/or ground at near-horizontal angles. Given the high sensitivity of specular reflections to the 3-D scene geometry, obtaining accurate DHRs for such highly specular materials in complex, real-world scenes would require extremely accurate modeling of the scene objects and viewing geometry.

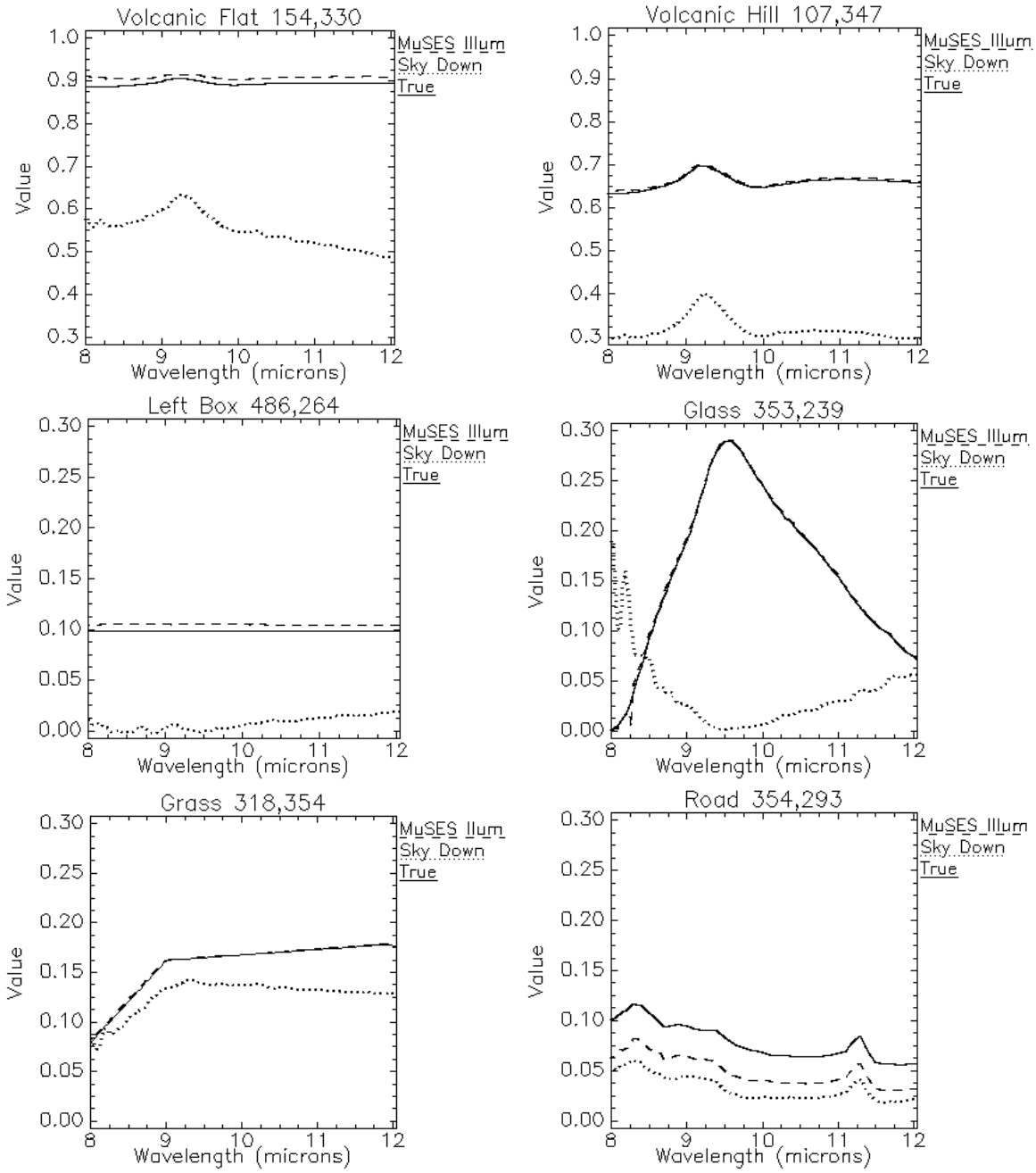

Figure 2. DHR results from FLAASH-IR and comparisons with true (input) spectra.

The ragged pond water spectra retrieved using the MuSES D_e (Figure 3, at right) illustrates the indeterminacy problem discussed above. We ascribe its occurrence here to a combination of the specular reflection of the building in the water, which yields a large D_e, and the water's low temperature.

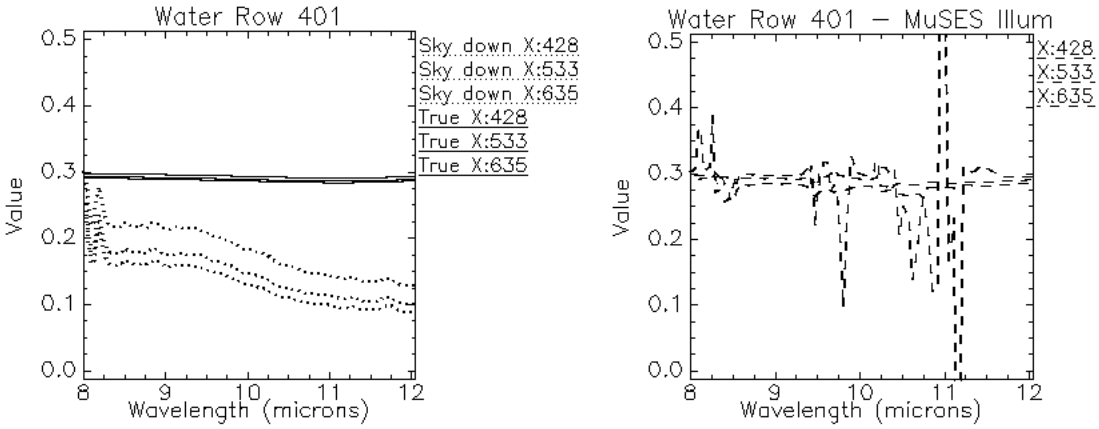

Figure 3. DHR results for three pond pixels from FLAASH-IR and comparison with true spectra.

SUMMARY AND CONCLUSIONS

The results of this study support the use of radiometrically accurate 3-D simulations of environmental illumination to assist in the retrieval, via temperature-emissivity separation (TES), of directional hemispherical reflectance and temperature properties of unknown surfaces in LWIR hyperspectral imagery. We caution that reflectance or emissivity retrievals become indeterminate as the brightness temperature of the illumination approaches that of the surface, an occurrence that is much more likely with horizontal or near-horizontal viewing than with near-nadir viewing. In these ill-determined cases, surface identification and characterization would be better achieved through comparisons between simulated and observed radiance spectra. On the other hand, the temperature retrievals are likely to remain accurate.

This study also provides support for FLAASH-IR's TES algorithm, which is based on an assumption of emissivity spectral smoothness. This algorithm is free from assumptions about absolute reflectance values or the presence or absence of specific materials in the scene. This makes it well-suited to situations where specularity generates elevated reflectances and a high degree of reflectance variability. However, with certain materials, and/or when the effect of the atmosphere is small, such as in dry conditions, an accurate absolute emissivity may not be retrieved with this TES method. We ascribe this to shallowness of the minimum in the objective function, σ^2, under those conditions. The TES errors with real HSI data have typically been in the direction of overestimated temperature (underestimated emissivity).[11] However, in this study we observed some errors in the opposite direction, such as with the road pixel in Figure 3.

One advantage of performing TES is the convenience of making direct comparisons with reflectance spectral libraries, without needing to carry along atmospheric information for a material radiance simulation. Another advantage is that the retrieval of surface temperature, even if it is only a rough estimate, greatly constrains the range of simulations to consider. Finally, TES can address deficiencies in an initial scene model, which is unlikely to perfectly match real surface temperatures. For example, TES performed on the measured HSI data could be used to retrieve background temperatures that refine the scene model and speed its convergence to the real scene properties. Our observation that the FLAASH-IR temperature retrievals were not very sensitive to the illumination suggests that simulation/retrieval/refinement iterations would converge rapidly.

ACKNOWLEDGEMENTS

This work was funded by Spectral Sciences, Inc. and Thermoanalytics, Inc. The MODTRAN® trademark is being used with the express permission of the owner, the United States of America, as represented by the United States Air Force.

REFERENCES

[1] Hernandez-Baquero, E.D. and Schott, J.R., "Atmospheric compensation for surface temperature and emissivity separation," Proc. SPIE Algorithms for Multispectral, Hyperspectral, and Ultraspectral Imagery VI 4049, 400-410 (2000).

[2] Borel, C.C., "ARTEMISS – an Algorithm to Retrieve Temperature and Emissivity from Hyper-Spectral Thermal Image Data," 28th Annual GOMACTech Conference, Hyperspectral Imaging Session, Los Alamos National Lab. Rpt. No. LA-UR-027907 (2003).

[3] Adler-Golden, S.M., Conforti, P., Gagnon, M., Tremblay, P. and Chamberland, M., "Long-wave infrared surface reflectance spectra retrieved from Telops Hyper-Cam imagery," Proc. SPIE Algorithms and Technologies for Multispectral, Hyperspectral, and Ultraspectral Imagery XX 90880, doi:10.1117/12.2050446 (2014a).

[4] Adler-Golden, S.M., Conforti, P., Gagnon, M., Tremblay, P. and Chamberland, M., "Remote sensing of surface emissivity with the Telops Hyper-Cam," Proc. 6th WHISPERS Conference, Lausanne, 24-27 June (2014b).

[5] Young, S.J., Johnson. B.R, and Hackwell, J. A., "An In-scene Method for Atmospheric Compensation of Thermal Hyperspectral Data," J. Geophys. Res. Atmospheres, 204, ACH 14-1 – ACH 14-20 (2002).

[6] Johnson, K., Curran, A., Less, D., Levanen, D., Marttila, E., Gonda, T. and Jones, J., "MuSES: A New Heat and Signature Management Design Tool for Virtual Prototyping," Ninth Annual Ground Target Modeling & Validation Conference, Houghton, MI, August 1998.

[7] Sanders, J.S., Johnson, K.R., Curran, A.R., and Rynes, P.L., "Ground target infrared signature modeling with the multiservice electro-optic signature (MuSES) code," Proc. SPIE Targets and Backgrounds VI: Characterization, Visualization, and the Detection Process 4029, 197 (2000)

[8] Berk, A., Anderson, G.P., Acharya, P.K., Bernstein, L.S., Muratov, L., Lee, J., Fox, M.J., Adler-Golden, S.M., Chetwynd, J.H., Hoke, M.L., Lockwood, R.B., Cooley, T.W. and Gardner, J.A., "MODTRAN5: a Reformulated Atmospheric Band Model with Auxiliary Species and Practical Multiple Scattering Options," Proc. SPIE International Optical Society of Engineering 5655, 88 (2005).

[9] Sandford, B.P. and Robertson, D.C., "Infrared reflectance properties of aircraft paints," U.S. Air Force Philips Laboratory, Geophysics Directorate, Technical Report AFRL/VSBT ESC-94–1004 (August 1994).

[10] Jin, X. and Levine, R.Y., "Bidirectional Reflectance Distribution Function Effects in Ladar-based Reflection Tomography," Optical Society of America, Vol. 48, No. 21, Applied Optics (2009).

[11] Sundberg, R., Adler-Golden, S.M., and Conforti, P., "Long-wavelength infrared hyperspectral data "mining" at Cuprite, NV," Proc. SPIE 9611 Imaging Spectrometry XX, 961107 (2015).